J|A|C|S
ARTICLES
Published on Web 05/29/2004

Hybrid QM/MM Study of Thio Effects in Transphosphorylation Reactions: The Role of Solvation

Brent A. Gregersen,[†] Xabier Lopez,[‡] and Darrin M. York*,[†]

Contribution from the Department of Chemistry, University of Minnesota, 207 Pleasant Street SE, Minneapolis, Minnesota 55455-0431, and Kimika Fakultatea, Euskal Herriko Unibertsitatea, P.K. 1072, 20080 Donostia, Euskadi, Spain

Received December 18, 2003; E-mail: york@chem.umn.edu

Abstract: Transphosphorylation thio effects in solution are studied using hybrid QM/MM calculations with a *d*-orbital semiempirical Hamiltonian. Activated dynamics simulations were performed for a 3′ ribose-phosphate model in an explicit 20 Å sphere of TIP3P water surrounded by a solvent boundary potential, and free energy analysis was performed using the weighted histogram analysis method. Single thio-substitutions at all of the phosphoryl oxygen positions and a double thio-substitution at the nonbridging positions were considered. The reaction free energy profiles are compared with available experimental data, and the role of solvation on the barrier heights and reaction coordinate is discussed. These results provide an important step in the characterization of thio effects in reactions of biological phosphates that may aid in the interpretation of kinetic data and ultimately help to unravel the catalytic mechanisms of ribozymes.

1. Introduction

RNA catalysis is an area of tremendous current interest and is the focus of considerable experimental and theoretical work.[1−7] Insight gained from a fundamental understanding of the mechanism of ribozyme catalysis holds considerable promise in the design of new medical therapies that target genetic disorders,[8−10] as well as the development of new biotechnology.[11−16] A variety of experimental methods have been used to study the cleavage of phosphodiester bonds by ribozymes[17−21] as well as the nonenzymatic pathways for the transphosphorylation and hydrolysis of RNA and related model phosphate systems in solution.[5−7] One method to probe the mechanism of ribozymes is to introduce site-specific chemical modifications,[14,22−26] from which mechanistic inferences can be made from the measured change in reaction rate. A commonly

[†] University of Minnesota.
[‡] Euskal Herriko Unibertsitatea.

(1) Herschlag, D.; Eckstein, F.; Cech, T. R. The importance of being ribose at the cleavage site in the tetrahymena ribozyme reaction. *Biochemistry* **1993**, *32*, 8312−8321.
(2) Heidenreich, O.; Benseler, F.; Fahrenholz, A.; Eckstein, F. High activity and stability of hammerhead ribozymes containing 2′-modified pyrimidine nucleosides and phosphorothioates. *J. Biol. Chem.* **1994**, *269*, 2131−2138.
(3) Beigelman, L.; Mcswiggen, J. A.; Draper, K. G.; Gonzalez, C.; Jensen, K.; Karpeisky, A. M.; Modak, A. S.; Matulic-Adamic, J.; Direnzo, A. B.; Haeberli, P.; Sweedler, D.; Tracz, D.; Grimm, S.; Wincott, F. E.; Thackray, V. G.; Usman, N. Chemical modification of hammerhead ribozymes. *J. Biol. Chem.* **1995**, *270*, 25702−25708.
(4) Scott, W. G. Biophysical and biochemical investigations of RNA catalysis in the hammerhead ribozyme. *Q. Rev. Biophys.* **1999**, *32*, 241−294.
(5) Perreault, D. M.; Anslyn, E. V. Unifying the current data on the mechanism of cleavage-transesterification of RNA. *Angew. Chem., Int. Ed. Engl.* **1997**, *36*, 432−450.
(6) Zhou, D.-M.; Taira, K. The hydrolysis of RNA: From theoretical calculations to the hammerhead ribozyme-mediated cleavage of RNA. *Chem. Rev.* **1998**, *98*, 991−1026.
(7) Oivanen, M.; Kuusela, S.; Lönnberg, H. Kinetics and mechanisms for the cleavage and isomerization of the phosphodiester bonds of RNA by Brønsted acids and bases. *Chem. Rev.* **1998**, *98*, 961−990.
(8) Hughes, M. D.; Hussain, M.; Nawaz, Q.; Sayyed, P.; Akhtar, S. The cellular delivery of antisense oligonucleotides and ribozymes. *DDT* **2001**, *6*, 313−315.
(9) Usman, N.; Beigelman, L.; McSwiggen, J. A. Hammerhead ribozyme engineering. *Curr. Opin. Struct. Biol.* **1996**, *1*, 527−533.
(10) Uhlmann, E.; Peyman, A. Antisense oligonucleotides: a new therapeutic principle. *Chem. Rev.* **1990**, *90*, 543−584.
(11) Silverman, S. K. Rube Goldberg goes (ribo)nuclear? Molecular switches and sensors made from RNA. *RNA* **2003**, *9*, 377−383.
(12) Sekella, P. T.; Rueda, D.; Walter, N. G. A biosensor for theophylline based on fluorescence detection of ligand-induced hammerhead ribozyme cleavage. *RNA* **2002**, *8*, 1242−1252.
(13) Soukup, G. A.; Breaker, R. R. Nucleic acid molecular switches. *Trends Biotechnol.* **1999**, *17*, 469−476.
(14) Puerta-Fernández, E.; Romero-López, C.; Barroso-Deljesus, A.; Berzal-Herranz, A. Ribozymes: Recent advances in the development of RNA tools. *FEMS Microbiol. Rev.* **2003**, *27*, 75−97.
(15) Cech, T. R. Ribozyme engineering. *Curr. Opin. Struct. Biol.* **1992**, *2*, 605−609.
(16) Breaker, R. R. In vitro selection of catalytic polynucleotides. *Chem. Rev.* **1997**, *97*, 371−390.
(17) Scott, W. G.; Klug, A. Ribozymes: Structure and mechanism in RNA catalysis. *Trends Biochem. Sci.* **1996**, *21*, 220−224.
(18) Scott, W. G. RNA catalysis. *Curr. Opin. Struct. Biol.* **1998**, *8*, 720−726.
(19) Scott, W. G. RNA structure, metal ions, and catalysis. *Curr. Opin. Struct. Biol.* **2000**, *3*, 705−709.
(20) Fedor, M. J. The role of metal ions in RNA catalysis. *Curr. Opin. Struct. Biol.* **2002**, *12*, 289−295.
(21) Doherty, E. A.; Doudna, J. A. Ribozyme structures and mechanisms. *Annu. Rev. Biophys. Biomol. Struct.* **2001**, *30*, 457−475.
(22) Herschlag, D.; Piccirilli, J. A.; Cech, T. R. Ribozyme-catalyzed and nonenzymic reactions of phosphate diesters: Rate effects upon substitution of sulfur for a nonbridging phosphoryl oxygen atom. *Biochemistry* **1991**, *30*, 4844−4854.
(23) Usman, N.; Cedergren, R. Exploiting the chemical synthesis of RNA. *Trends Biochem. Sci.* **1992**, *17*, 334−339.
(24) Catrina, I. E.; Hengge, A. C. Comparisons of phosphorothioate and phosphate monoester transfer reactions: Activation parameters, solvent effects, and the effect of metal ions. *J. Am. Chem. Soc.* **1999**, *121*, 2156−2163.
(25) Smith, J. S.; Nikonowicz, E. P. Phosphorothioate substitution can substantially alter RNA conformation. *Biochemistry* **2000**, *39*, 5642−5652.
(26) Catrina, I. E.; Hengge, A. C. Comparisons of phosphorothioate with phosphate transfer reactions for a monoester, diester, and triester: Isotope effect studies. *J. Am. Chem. Soc.* **2003**, *125*, 7546−7552.

10.1021/ja031815l CCC: $27.50

applied modification involves the substitution of one or more oxygens at the reactive phosphate with sulfur.[6,22,24,26,27] A subsequent change in the reaction rate is called a thio effect and can provide insight into the role these positions play in the biological reaction. Theoretical methods offer a potentially powerful tool to aid in the mechanistic interpretation of experimental kinetic data and provide additional atomic-level insight into the structural and chemical reaction dynamics.[28−31]

Quantum electronic structure methods offer a means to study chemical reactions of biological phosphates. These systems have been the focus of theoretical studies in the gas phase,[32−35] in solution[36−42] (including *ab initio* studies of the nature of associative and dissociative paths[43−45]), and in enzymatic environments.[46−48] Conventional electronic structure methods alone are limited by the size of the systems that can be routinely handled and the degree to which configurational space can be sampled.

The nature of most biochemical reactions is such that only a small, localized chemically reactive region requires a high-level quantum mechanical treatment. The environment plays a critical role in stabilizing the reaction, but this influence does not require complex electronic structure methods to accurately model. Consequently, a particularly useful strategy to study chemical reactions in complex aqueous biological environments is to perform activated molecular dynamics simulations with hybrid quantum mechanical/molecular mechanical (QM/MM) potentials[49−52] to derive reaction free energy profiles for different possible mechanistic pathways. A key factor in these simulations is to employ quantum methods that are sufficiently accurate and efficient to derive reliable free energy results. The development of new quantum models for QM/MM simulations of biological reactions is an area of tremendous importance and is the focus of considerable research effort.

Scheme 1. In-Line Dianionic Mechanism of Transphosphorylation

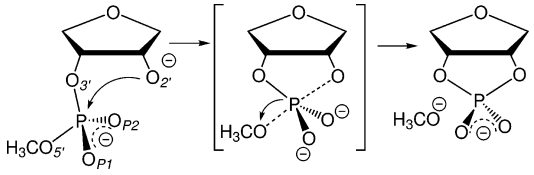

In this work, a hybrid QM/MM approach is used to study the mechanisms of alkaline transphosphorylation thio effects of a model biological system in solution (Scheme 1). Single thio-substitutions in the bridging and nonbridging phosphoryl oxygen positions are studied in addition to a double nonbridging thio-substitution. The present paper extends recently communicated work[53] by reporting new results using a more rigorous treatment of solvent−solvent electrostatic interactions and inclusion of a comprehensive characterization of the role of solvent stabilization on the reaction path and free energy profiles. These results provide detailed insight into the nature of thio effects on transphosphorylation reactions of biological phosphates.

2. Methods

Activated Dynamics Simulations. A 20 Å sphere of equilibrated TIP3P waters[54] was centered about the center of mass of the sugar-phosphodiester or thio-substituted analogue (the solute). Water molecules less than 2.8 Å from the solute were removed. The resulting system containing 1076 water molecules and 21 solute atoms was partitioned into multiple zones to perform stochastic boundary molecular dynamics.[55,56] No explicit counterions were included, resulting in a −2 charge of the complete system. Molecules in the reaction zone from 0 to 16 Å were surrounded by a buffer zone from 16 to 20 Å. To prevent excessive drift of the solute due to diffusion over long time scales, a

(27) Breslow, R.; Chapman, W. H., Jr. On the mechanism of action of ribonuclease A: Relevance of enzymatic studies with a *p*-nitrophenylphosphate ester and a thiophosphate ester. *Proc. Natl. Acad. Sci. U.S.A.* **1996**, *93*, 10018−10021.
(28) Warshel, A. *Computer Modeling of Chemical Reactions in Enzymes and Solutions*; John Wiley and Sons: New York, 1991.
(29) Karplus, M. Aspects of protein reaction dynamics: Deviations from simple behavior. *J. Phys. Chem. B* **2000**, *104*, 11−27.
(30) Friesner, R. A.; Beachy, M. D. Quantum mechanical calculations on biological systems. *Curr. Opin. Struct. Biol.* **1998**, *8*, 257−262.
(31) Warshel, A. Computer simulations of enzyme catalysis: Methods, progress, and insights. *Annu. Rev. Biophys. Biomol. Struct.* **2003**, *32*, 425−443.
(32) Lim, C.; Karplus, M. Nonexistence of dianionic pentacovalent intermediates in an ab initio study of the base-catalysed hydrolysis of ethylene phosphate. *J. Am. Chem. Soc.* **1990**, *112*, 5872−5873.
(33) Uchimaru, T.; Tanabe, K.; Nishikawa, S.; Taira, K. Ab initio studies of a marginally stable intermediate in the base-catalyzed methanolysis of dimethyl phosphate and nonexistence of the stereoelectronically unfavorable transition state. *J. Am. Chem. Soc.* **1991**, *113*, 4351−4353.
(34) Lim, C.; Tole, P. Concerted hydroxyl ion attack and pseudorotation in the base-catalyzed hydrolysis of methyl ethylen phosphate. *J. Phys. Chem.* **1992**, *96*, 5217−5219.
(35) Mercero, J. M.; Barrett, P.; Lam, C. W.; Fowler, J. E.; Ugalde, J. M.; Pedersen, L. G. Quantum mechanical calculations on phosphate hydrolysis reactions. *J. Comput. Chem.* **2000**, *21*, 43−51.
(36) Dejaegere, A.; Lim, C.; Karplus, M. Dianionic pentacoordinate species in the base-catalyzed hydrolysis of ethylene and dimethyl phosphate. *J. Am. Chem. Soc.* **1991**, *113*, 4353−4355.
(37) Dejaegere, A.; Karplus, M. Hydrolysis rate difference between cyclic and acyclic phosphate esters: Solvation versus strain. *J. Am. Chem. Soc.* **1993**, *115*, 5316−5317.
(38) Tole, P.; Lim, C. New insights into the base-catalyzed hydrolysis of methyl ethylene phosphate. *J. Phys. Chem.* **1993**, *97*, 6212−6219.
(39) Tole, P.; Lim, C. The significance of electrostatic effects in phospho-ester hydrolysis. *J. Am. Chem. Soc.* **1994**, *116*, 3922−3931.
(40) Chang, N.; Lim, C. An ab initio study of nucleophilic attack of trimethyl phosphate: Factors influencing site reactivity. *J. Phys. Chem. A* **1997**, *101*, 8706−8713.
(41) López, X.; Dejaegere, A.; Karplus, M. Solvent effects on the reaction coordinate of the hydrolysis of phosphates and sulfates: Application of Hammond and anti-Hammond postulates to understand hydrolysis in solution. *J. Am. Chem. Soc.* **2001**, *123*, 11755−11763.
(42) López, X.; Schaefer, M.; Dejaegere, A.; Karplus, M. Theoretical evaluation of pK_a in phosphoranes: Implications for phosphate ester hydrolysis. *J. Am. Chem. Soc.* **2002**, *124*, 5010−5018.
(43) Florián, J.; Warshel, A. A fundamental assumption about OH-attack in phosphate ester hydrolysis is not fully justified. *J. Am. Chem. Soc.* **1997**, *119*, 5473−5474.
(44) Florián, J.; Warshel, A. Phosphate ester hydrolysis in aqueous solution: Associative versus dissociative mechanisms. *J. Phys. Chem. B* **1998**, *102*, 719−734.
(45) Hu, C.-H.; Brinck, T. Theoretical studies of the hydrolysis of the methyl phosphate anion. *J. Phys. Chem. A* **1999**, *103*, 5379−5386.
(46) Glennon, T. M.; Warshel, A. Energetics of the catalytic reaction of Ribonuclease A: A computational study of alternative mechanisms. *J. Am. Chem. Soc.* **1998**, *120*, 10234−10247.
(47) Jones, G. A.; Carpenter, B. K.; Paddon-Row, M. N. Application of trajectory surface hopping to the study of intramolecular electron transfer in polyatomic organic systems. *J. Am. Chem. Soc.* **1998**, *120*, 5488−5498.
(48) López, X.; York, D. M.; Dejaegere, A.; Karplus, M. Theoretical studies on the hydrolysis of phosphate diesters in the gas phase, solution, and RNase A. *Int. J. Quantum Chem.* **2002**, *86*, 10−26.
(49) Warshel, A.; Levitt, M. Theoretic studies of enzymatic reactions: Dielectric electrostatic and steric stabilization in the reaction of lysozyme. *J. Mol. Biol.* **1976**, *103*, 227−249.
(50) Åqvist, J.; Warshel, A. Simulation of enzyme-reactions using valence-bond force-fields and other hybrid quantum-classical approaches. *Chem. Rev.* **1993**, *93*, 2523−2544.
(51) Gao, J. Methods and applications of combined quantum mechanical and molecular mechanical potentials. *Rev. Comput. Chem.* **1995**, *7*, 119−185.
(52) Gao, J.; Truhlar, D. G. Quantum mechanical methods for enzyme kinetics. *Annu. Rev. Phys. Chem.* **2002**, *53*, 467−505.
(53) Gregersen, B. A.; López, X.; York, D. M. Hybrid QM/MM study of thio effects in transphosphorylation reactions. *J. Am. Chem. Soc.* **2003**, *125*, 7178−7179.
(54) Jorgensen, W. L.; Chandrasekhar, J.; Madura, J. D.; Impey, R. W.; Klein, M. L. Comparison of simple potential functions for simulating liquid water. *J. Chem. Phys.* **1983**, *79*, 926−935.
(55) Brooks, C. L., III; Karplus, M. Deformable stochastic boundaries in molecular dynamics. *J. Chem. Phys.* **1983**, *79*, 6312−6325.
(56) Brooks, C. L., III; Brunger, A.; Karplus, M. Active site dynamics in protein molecules: A stochastic boundary molecular dynamics approach. *Biopolymers* **1985**, *24*, 843−865.

weak harmonic restraint ($E_{cm} = {}^1/_2 k_{cm}(r_{cm})^2$) on the center of mass of the solute was introduced, where k_{cm} was chosen to be 21 kcal mol^{-1} Å^{-2} (i.e., 1 kcal/mol/atom) and r_{cm} is the location of the solute center-of-mass relative to the origin. The reaction zone was propagated with Hamiltonian dynamics, whereas water molecules in the buffer zone were propagated with Langevin dynamics ($\tau = 62.0$ ps^{-1}) to serve as a constant-temperature bath (300 K), and a deformable boundary potential was used to reproduce the containment effect of bulk solvent outside the buffer zone.[56]

Quantum Treatment of Solute. The quantum system consisted of the sugar-phosphodiester or corresponding thio-substituted phosphorothioate depicted in Scheme 1. The entire solute was treated quantum mechanically, and there was no need for special consideration of a QM/MM boundary that cut across covalent bonds (because no such boundary existed). The quantum model employed was the semiempirical MNDO/d Hamiltonian[57] interfaced with CHARMM.[58] In this work, no semiempirical parameter modifications to the MNDO/d method were introduced. The solute van der Waals parameters were taken from the CHARMM c27 force field parameters for nucleic acids.[59] The van der Waals radii for the sulfur atoms were taken to be identical to the parameters for the sulfur atom types of cysteine ($\epsilon = 0.45$ kcal/mol, $R_0 = 2.0$ Å).

Semiempirical quantum models are frequently used in hybrid QM/MM simulations of biochemical reactions where dynamic sampling of a complex environment is essential,[60] including transphosphorylation reactions of biological phosphates.[53] The use of *d*-orbitals has been demonstrated to be extremely important to model second-row elements such as phosphorus and sulfur,[57] and in particular for hypervalent species such as phosphorane and thiophosphorane transition states/intermediates in the present work.[61] Perhaps the most significant limitation of the MNDO/d method is the inability to accurately model hydrogen-bonding and proton-transfer reactions; however, for the dianionic systems studied here, these interactions are not present within the quantum subsystem. The MNDO/d method has been demonstrated previously[61] to be reliable relative to density-functional calculations of biological phosphates and phosphoranes[62] and considerably superior to other semiempirical methods that lack a *d*-orbital description.

Umbrella Sampling. Umbrella sampling[63] was used to collect statistics over the reaction coordinate range (-3.1 Å $\le r_2 - r_1 \le 3.7$ Å, where r_1 and r_2 are the P···O$_{2'}$ and P···O$_{5'}$ distances, respectively). A harmonic restraint $E_{res} = {}^1/_2 k(r_2 - r_1 - r_c)^2$ was added to the total energy, where k is a force constant (100 kcal mol^{-1} Å^{-2}) and r_c is the equilibrium reaction coordinate value for the umbrella potential of a particular sampling window. A total of 35 windows spaced 0.2 Å apart were used to collect overlapping statistics. Each window was equilibrated at 300 K for 10 ps, followed by 50 ps of sampling. A 0.5 fs integration time step was used to propagate the system. No electrostatic or van der Waals cutoffs were used in this study for either the water−water (MM−MM) or the water−solute (MM−QM) nonbonded interactions. The SHAKE algorithm[64] was used to constrain the internal water geometries. Reaction coordinate and energy statistics were saved after each step, resulting in 100 000 data points per window and 3.5 million total points to construct each free energy profile.

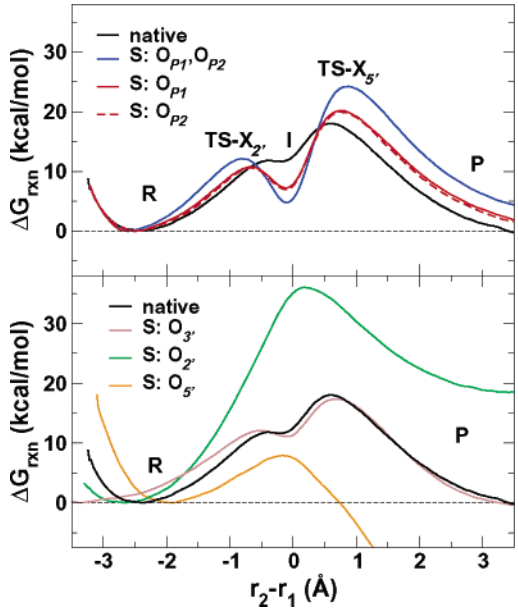

Figure 1. Free energy profiles for native and thio-substituted transphosphorylation reactions.

Free Energy Profiles. Free energy profiles as a function of the $r_2 - r_1$ coordinate were calculated using the weighted histogram analysis method (WHAM)[65] with a 0.02 Å bin spacing. The statistics needed to generate the free energy profiles were collected using a modified version of CHARMM c27[58] interfaced with MNDO97.[66] The CHARMM program was modified to output the reaction coordinate value and energy components at each time step.

The value of the r_1 = P−X$_{2'}$ and r_2 = P−X$_{5'}$ distances at the transition state were determined as follows. First, the average reaction coordinate (r_c) value, along with the corresponding average r_1 and r_2 values, were determined for each of the 31 umbrella windows. The average r_1 and r_2 values were then placed on separate cubic splines[67] with common r_c values. The value of the reaction coordinate at the rate limiting transition state was obtained from the free energy profiles and subsequently used to determine individual interpolated values for r_1 and r_2.

Overall, the inclusion of *d*-orbitals and a full (no cutoff) electrostatic description, combined with dense umbrella sampling along the reaction coordinate and weighted histogram analysis, offers a protocol that is able to produce stable, converged free energy profiles for the dianionic reactions studied in the present work.

3. Results

3.1. Reaction Profiles. Figure 1 shows the free energy profiles for the native (unsubstituted) and sulfur-substituted in-line dianionic attack mechanism of transphosphorylation. Relative free energy values for the stationary points on the free energy surface are compared in Table 1, and their corresponding average geometrical data are summarized in Table 2.

(57) Thiel, W.; Voityuk, A. A. Extension of MNDO to d orbitals: Parameters and results for the second-row elements and for the zinc group. *J. Phys. Chem.* **1996**, *100*, 616−626.
(58) Brooks, B. R.; Bruccoleri, R. E.; Olafson, B. D.; States, D. J.; Swaminathan, S.; Karplus, M. Charmm: A program for macromolecular energy minimization and dynamics calculations. *J. Comput. Chem.* **1983**, *4*, 187−217.
(59) Foloppe, N.; Mackerell, A. D., Jr. All-atom empirical force field for nucleic acids: I. Parameter optimization based on small molecule and condensed phase macromolecular target data. *J. Comput. Chem.* **2000**, *21*, 86−104.
(60) Garcia-Viloca, M.; Gao, J.; Karplus, M.; Truhlar, D. G. How enzymes work: Analysis by modern rate theory and computer simulations. *Science* **2004**, *303*, 186−195.
(61) López, X.; York, D. M. Parametrization of semiempirical methods to treat nucleophilic attacks to biological phosphates: AM1/d parameters for phosphorus. *Theor. Chem. Acc.* **2003**, *109*, 149−159.
(62) Range, K.; Mcgrath, M. J.; López, X.; York, D. M. The structure and stability of biological metaphosphate, phosphate, and phosphorane compounds in the gas phase and in solution. *J. Am. Chem. Soc.* **2004**, *126*, 1654−1665.
(63) Torrie, G. M.; Valleau, J. P. Monte Carlo free energy estimates using non-Boltzmann sampling: Application to the sub-critical Lennard-Jones fluid. *Chem. Phys. Lett.* **1974**, *28*, 578−581.
(64) Ryckaert, J. P.; Ciccotti, G.; Berendsen, H. J. C. Numerical integration of the Cartesian equations of motion of a system with constraints: Molecular dynamics of *n*-alkanes. *J. Comput. Phys.* **1977**, *23*, 327−341.
(65) Kumar, S.; Bouzida, D.; Swendsen, R.; Kollman, P.; Rosenberg, J. The weighted histogram analysis method for free-energy calculations on biomolecules 1: The method. *J. Comput. Chem.* **1992**, *13*, 1011−1021.
(66) Thiel, W. *Program MNDO97*; University of Zurich, 1998.
(67) Press, W. H.; Teukolsky, S. A.; Vetterling, W. T.; Flannery, W. P. *Numerical Recipes in Fortran*, 2nd ed.; Cambridge University Press: Cambridge, 1992.

Table 1. Comparison of Thermodynamic Data for the In-Line Dianionic Mechanism of Transphosphorylation Reactions in Solution[a]

reaction	$\Delta G_{X_{2'}}^{\ddagger}$	ΔG_I	$\Delta G_{X_{5'}}^{\ddagger}$	$\Delta\Delta G^{\ddagger}$	$\Delta G_{I_{col}}$	k_O/k_S
native	11.8	11.6	**18.0**	6.2	0.2	
S: O_{P1}	10.7	7.2	**20.2**	9.5	3.5	40.2
S: O_{P2}	10.6	6.9	**19.9**	9.3	3.7	24.3
S: O_{P1},O_{P2}	12.1	4.8	**24.2**	12.1	7.3	3.31×10^3
S: $O_{3'}$	12.1	11.1	**17.3**	5.2	1.0	0.309
S: $O_{2'}$			**36.0**			1.32×10^{13}
S: $O_{5'}$	**7.9**					4.34×10^{-8}

[a] Relative free energies (kcal/mol) with respect to reactants at 300 K along the reaction coordinate for the dianionic in-line attack mechanism of sugar-phosphates and sugar-phosphorothioates in solution. The rate-limiting TS is indicated in boldface font. Shown also are the relative free energies of the transition states ($\Delta\Delta G^{\ddagger}$), the free energy barriers for collapse of the intermediate ($\Delta G_{I_{col}}$), and the estimated thio effects (k_O/k_S). See text for further details.

Table 2. Comparison of Geometric Data for the In-Line Dianionic Mechanism of Transphosphorylation Reactions in Solution[a]

	$TS_{X_{2'}}$			I			$TS_{X_{5'}}$		
reaction	r_1	r_2	θ	r_1	r_2	θ	r_1	r_2	θ
native	2.19	1.79	165.5	2.01	1.83	165.0	1.80	2.40	164.1
S: O_{P1}	2.38	1.73	165.0	1.91	1.80	165.6	1.77	2.52	162.0
S: O_{P2}	2.40	1.73	164.2	1.91	1.80	165.1	1.77	2.52	162.2
S: O_{P1},O_{P2}	2.49	1.71	163.5	1.88	1.77	165.0	1.76	2.63	160.4
S: $O_{3'}$	2.31	1.77	166.5	1.94	1.85	163.6	1.78	2.47	165.2
S: $O_{2'}$							2.27	2.45	165.2
S: $O_{5'}$	2.42	2.25	165.1						

[a] Geometric parameters include $r_1 = P-X_{2'}$ and $r_2 = P-X_{5'}$ distances (Å), and $\theta = X_{2'}-P-X_{5'}$ angle (deg).

The two transition states characteristic of the predominantly associative in-line nucleophilic attack correspond to the formation of the endocyclic $P-X_{2'}$ bond and cleavage of the exocyclic $P-X_{5'}$ bond (where "X" is either oxygen or sulfur). These transition states are designated $TS_{X_{2'}}$ and $TS_{X_{5'}}$, respectively. In the case where both of these transition states are present (indicative of an $A_N + D_N$-type mechanism in IUPAC nomenclature[68]), there exists a stable (or metastable) phosphorane intermediate along the reaction path that connects the transition states and is designated I. Substitution at the $O_{5'}$ or $O_{2'}$ position results in an asynchronous concerted reaction (A_ND_N-type mechanism) that proceeds through a single transition state. The degree of association for each of the stationary points is depicted in Figure 2, which illustrates the various reaction paths as a function of the $r_1 = P-X_{2'}$ and $r_2 = P-X_{5'}$ distances.

Other quantities derivable from the free energy profiles that are of interest for discussion include the relative heights of the transition states

$$\Delta\Delta G^{\ddagger} \equiv \Delta G_{X_{5'}}^{\ddagger} - \Delta G_{X_{2'}}^{\ddagger} \qquad (1)$$

(where $\Delta G_{X_{2'}}^{\ddagger}$ and $\Delta G_{X_{5'}}^{\ddagger}$ are the free energy barriers for $TS_{X_{2'}}$ and $TS_{X_{5'}}$, respectively), the (lowest) barrier to collapse of the intermediate

$$\Delta G_{I_{col}} \equiv \mathrm{MIN}(\Delta G_{X_{2'}}^{\ddagger}, \Delta G_{X_{5'}}^{\ddagger}) - \Delta G_I \qquad (2)$$

(where ΔG_I is the free energy of the intermediate I), and an estimated "thio effect"[22] given by the ratio of rate constants

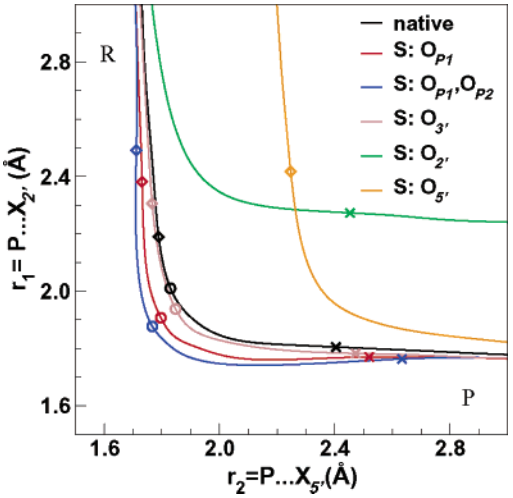

Figure 2. Plot of the average values of r_1 and r_2 for each umbrella sampling window. Stationary points on the free energy profile are markers for: $TS_{X_{2'}}$ (◇), intermediate (○), and $TS_{X_{5'}}$ (×).

derived from the rate-controlling barriers (assuming unit transmission coefficients and no tunneling) for the unsubstituted reaction (k_O) and the sulfur-substituted reaction (k_S),

$$k_O/k_S = e^{(\Delta G_O^{\ddagger} - \Delta G_S^{\ddagger})/k_B T} \qquad (3)$$

where $\Delta G_O^{\ddagger}$ and $\Delta G_S^{\ddagger}$ are the rate-controlling free energy barriers for the unsubstituted and sulfur-substituted reactions, respectively, k_B is the Boltzmann constant, and T is the absolute temperature. The values of these quantities for each reaction are listed in Table 1.

3.2. Solvent Structure. Solvation has a large stabilization effect on the transition states for transphosphorylation and hydrolysis reactions under alkaline conditions that involve association of anionic reactants.[36−45] It has been demonstrated, for example, that solvation is the dominant influence on the observed enhanced reactivity toward hydrolysis of cyclic versus acyclic phosphates.[37] For dianionic transphosphorylation reactions, theoretical calculations predict solvation lowers the rate-limiting activation barrier by around 50 kcal/mol relative to the reaction in the gas phase.[33,69,70]

To assess the role of solvation on the reaction coordinate for in-line dianionic attack, the radial distribution functions of water oxygens around key atoms of the reactive phosphate have been calculated separately for the reactant minima, rate-limiting transition states, and product minima. The radial distribution functions (rdf's) are denoted $g_{XY}^{S}(r)$ where the subscript XY refers to the distribution of Y atoms around X atoms, and the superscript S ("structure") refers to the reactant (R), rate-limiting transition state (TS), or product (P) states. Key properties derivable from the radial distribution functions are summarized for each of the reactions in Table 3. A summary of the statistics for all of the radial distribution functions of water around the various phosphoryl positions is provided as Supporting Information.

(68) Guthrie, R. D.; Jencks, W. P. IUPAC recommendations for the representation of reaction mechanisms. *Acc. Chem. Res.* **1989**, *22*, 343−349.

(69) Florián, J.; Åqvist, J.; Warshel, A. On the reactivity of phosphate monoester dianions in aqueous solution: Brønsted linear free-energy relationships do not have a unique mechanistic interpretation. *J. Am. Chem. Soc.* **1998**, *120*, 11524−11525.

(70) López, X.; York, D. M.; Dejaegere, A.; Karplus, M. Nucleophilic attack on phosphate diesters: A density functional dataset for in-line reactivity. **2004**, in preparation.

Table 3. Radial Distribution Statistics of Water Oxygens (O_W) around the 2′, P, and 5′ Positions in the Reactant, Rate-Limiting Transition State, and Product States for In-Line Dianionic Transphosphorylation Reactions in Solution

reaction	r_{max1}	$g(r)_{max1}$	r_{min1}	$g(r)_{min1}$	CN_1	$\langle r \rangle_1$	$\sqrt{\langle \sigma_r^2 \rangle_1}$
			Reactant $X_{2'}-O_W$				
native	2.8	3.39	3.6	0.26	4.7	2.95	1.69
S: O_{P1}	2.8	3.34	3.5	0.25	4.5	2.92	1.65
S: O_{P2}	2.8	3.18	3.6	0.26	4.6	2.94	1.68
S: O_{P1}, O_{P2}	2.8	3.27	3.6	0.26	4.7	2.95	1.69
S: $O_{3'}$	2.8	3.13	3.7	0.26	4.7	2.99	1.74
S: $O_{2'}$	3.2	2.50	4.0	0.42	6.4	3.38	2.18
S: $O_{5'}$	2.8	3.28	3.6	0.26	4.4	2.94	1.68
			TS $P-O_W$				
native	3.9	2.32	4.8	0.46	11.7	4.07	2.92
S: O_{P1}	4.0	1.82	4.9	0.66	11.5	4.25	3.11
S: O_{P2}	4.0	1.74	5.2	0.67	14.0	4.45	3.34
S: O_{P1}, O_{P2}	4.3	1.43	5.4	0.75	15.2	4.85	3.76
S: $O_{3'}$	3.9	2.14	4.7	0.53	10.7	4.11	2.97
S: $O_{2'}$	3.9	2.19	4.9	0.50	11.6	4.15	3.02
S: $O_{5'}$	4.0	2.06	4.9	0.60	11.7	4.17	3.03
			Product $X_{5'}-O_W$				
native	2.8	3.87	3.4	0.35	5.1	2.90	1.63
S: O_{P1}	2.8	3.86	3.5	0.36	5.5	2.91	1.65
S: O_{P2}	2.8	3.79	3.5	0.36	5.2	2.92	1.65
S: O_{P1}, O_{P2}	2.8	3.65	3.5	0.33	5.3	2.93	1.66
S: $O_{3'}$	2.8	3.72	3.6	0.36	5.3	2.95	1.69
S: $O_{2'}$	2.8	3.69	3.4	0.39	5.1	2.91	1.64
S: $O_{5'}$	3.2	3.10	3.9	0.52	6.9	3.35	2.14

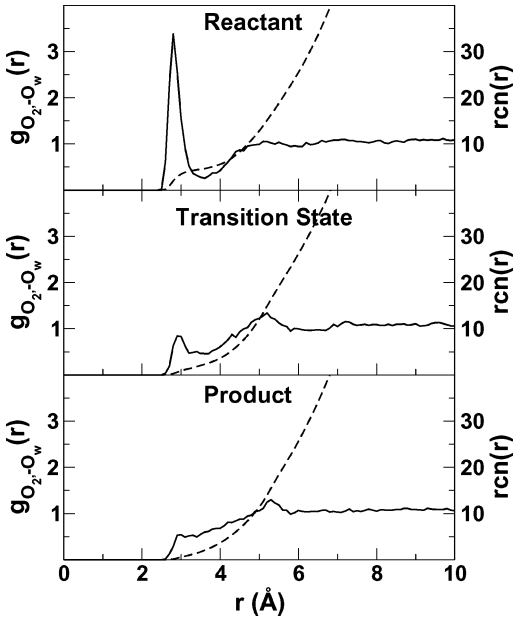

Figure 3. Radial distribution function and running coordination number (rcn) of water oxygens around 2′-oxygen at the reactant, transition state, and product for the native reaction.

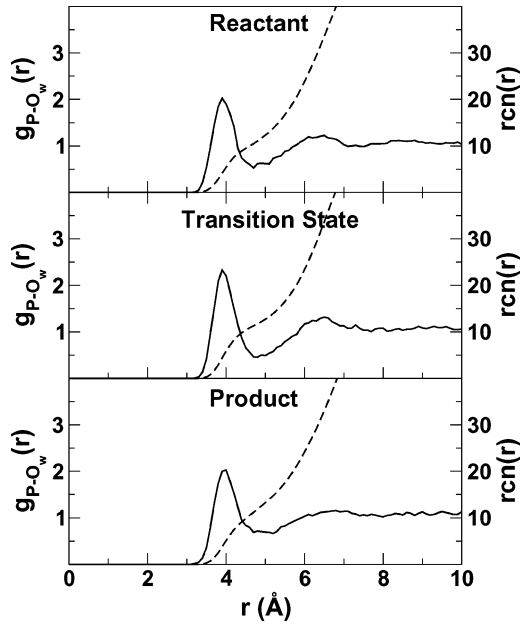

Figure 4. Radial distribution function and running coordination number (rcn) of water oxygens around phosphorus at the reactant, transition state, and product for the native reaction.

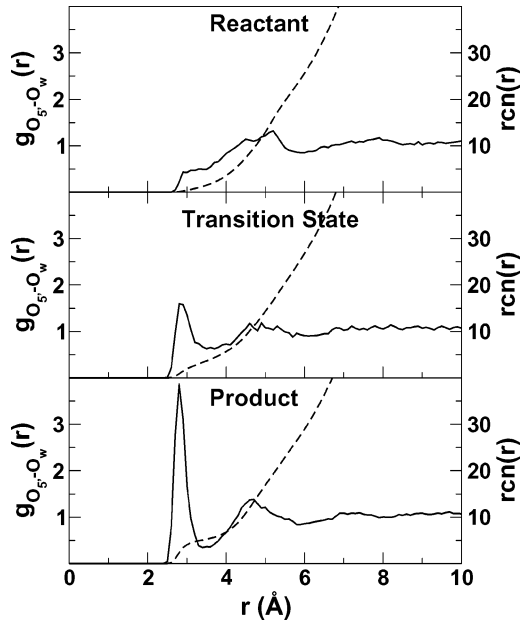

Figure 5. Radial distribution function and running coordination number (rcn) of water oxygens around 5′-oxygen at the reactant, transition state, and product for the native reaction.

All of the dianionic transphosphorylation reactions studied here involve the association of monoanionic reactants to form dianionic intermediates and transition states. Solvation plays a key role in the stabilization of these intermediates. (The solvation free energy, in the linear-response regime, is expected to vary in magnitude as the square of the total charge of the system. This suggests that the dianionic species should be considerably more solvent stabilized than the separated monoanionic species.) Figures 3−5 show the radial distribution functions of water oxygens around the nucleophile $O_{2'}^-$, phosphorus (P), and leaving group $O_{5'}^-$ positions, respectively, for the reactant, rate-limiting transition state, and product species.

Of the radial distribution functions presented, thio-substitutions at the nonbridging phosphoryl positions affect primarily the solvation around phosphorus in the transition state (Figure 7) and have little effect on the solvation of the $O_{2'}$ and $O_{5'}$ positions in the reactant and product states, respectively. Alternately, thio-substitution at the 2′, 3′, and 5′ positions most significantly affects the radial distribution functions of the reactant (Figure 6), transition state (Figure 7), and product (Figure 8), respectively.

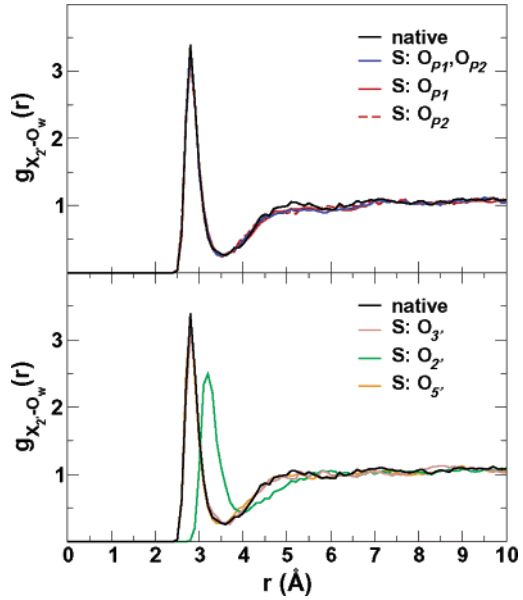

Figure 6. Radial distribution functions of water oxygens (O_W) around 2′ X (X = O or S) for the reactant state.

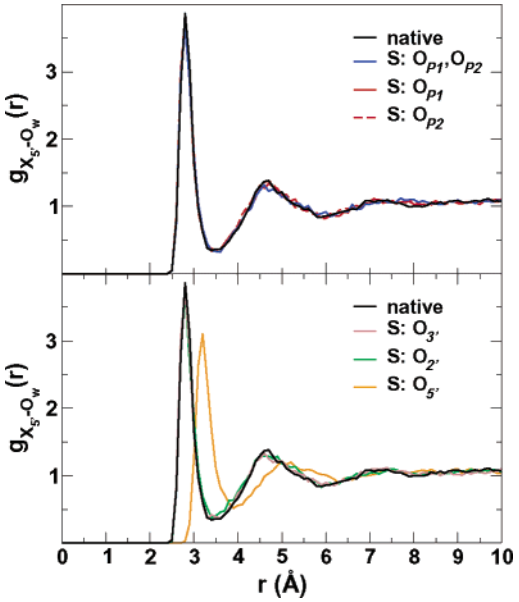

Figure 8. Radial distribution functions of water oxygens (O_W) around 5′ X (X = O or S) for the product state.

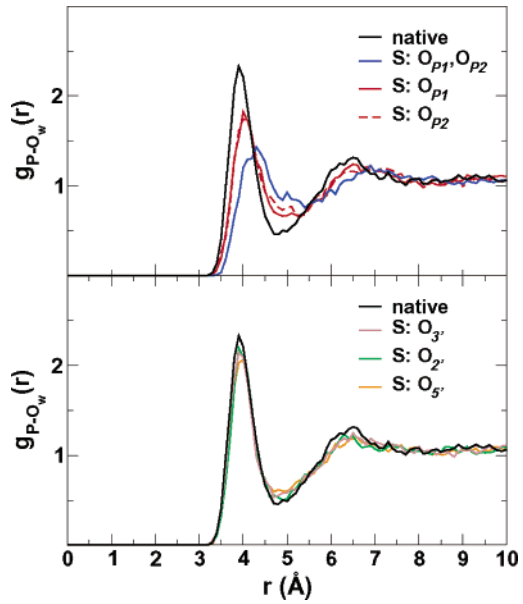

Figure 7. Radial distribution functions of water oxygens (O_W) around phosphorus (P) for the transition state.

4. Discussion

4.1. Free Energy Profiles. 4.1.1. Native (Unsubstituted) Reaction. The native (unsubstituted) reaction proceeds through two transition states corresponding to the formation of the P−$O_{2'}$ bond ($TS_{O_{2'}}$) and departure of the 5′-methoxy group ($TS_{O_{5'}}$). The rate-controlling step is the cleavage of the exocyclic P−$O_{5'}$ bond with a free energy barrier of 18.0 kcal/mol, which is higher than the endocyclic cleavage barrier by 6.2 kcal/mol. The transition states are separated by a kinetically insignificant intermediate with a barrier of only 0.2 kcal/mol to collapse back to the reactant. The calculated free energy profile under alkaline conditions is consistent with the experimentally supported hypothesis[5] that a dianionic oxyphosphorane cannot be distinguished kinetically from a transition state. The 2′,3′-cyclic phosphate, in the absence of an enhanced leaving group, can be readily detected only under alkaline conditions because of rapid acid-catalyzed hydrolysis to give 2′ or 3′-phosphates. Moreover, alkaline conditions disfavor isomerization of the 3′,5′ phosphate in RNA to give a 2′,5′ phosphate migration product[7] and prevent ^{18}O exchange between isotopically labeled water and ethylene phosphate, both reactions of which proceed via a pseudorotation mechanism. These experimental observations are consistent with the argument that a cyclic dianionic phosphorane is not sufficiently long-lived to undergo pseudorotation.

The rate-controlling transition state is a late transition state (Figure 2) with the exocyclic P−$O_{5'}$ bond nearly broken (2.39 Å). There is abundant experimental evidence from kinetic studies, including studies of primary leaving group kinetic isotope effects[71] and models with and without enhanced leaving groups,[6] in support of exocyclic cleavage as the rate-controlling step. The values for the axial $O_{2'}$−P−$O_{5'}$ angle are considerably distorted from an ideal value of 180° in a neutral phosphorane. The values range from 164.1° to 165.5° and indicate a slightly increased deviation from linearity as the reaction proceeds.

4.1.2. Substitution at the Nonbridging Phosphoryl Positions. Single substitution in the nonbridging positions raises the rate-controlling barrier relative to the native reaction by approximately 2 kcal/mol. The barrier to endocyclic bond formation is approximately 9.4 kcal/mol lower than the rate-controlling exocyclic cleavage barrier. A kinetically significant intermediate exists in a shallow free energy minima with a barrier to collapse to reactants of approximately 3.6 kcal/mol. These results suggest that alkaline transphosphorylation reactions show a considerable thio effect at the nonbridging phosphoryl positions. This result is in some contrast with experimental results for RNA analogues with nonbridging thio-substitutions that exhibit only modest thio effects.[7,72] The single substitution trends are all roughly linearly

(71) Hengge, A. C. Isotope effects in the study of phosphoryl and sulfuryl transfer reactions. *Acc. Chem. Res.* **2002**, *35*, 105−112.
(72) Almer, H.; Strömberg, R. Intramolecular transesterification in thiophosphate-analogues of an RNA-dimer. *Tetrahedron Lett.* **1991**, 32, 3723−3726.

propagated upon double sulfur substitution at the nonbridging phosphoryl positions. The rate-controlling barrier increases to 24.2 kcal/mol. The barrier to endocyclic bond formation is 12.1 kcal/mol lower than exocyclic cleavage, and the intermediate resides in a fairly deep kinetic well with a barrier of 7.3 kcal/mol to collapse to reactants. These results are consistent with experimental observations that phosphorothioates with double sulfur substitution at the nonbridging positions are much more resistant to hydrolysis.[6] However, the magnitude of the observed thio effects is again in some contrast with experimental results for doubly substituted, nonbridging phosphoryl positions.[73]

The existence of a stable dianionic thiophosphorane intermediate has important implications because, especially in the case of the dithiophosphorane, the lifetime may be sufficient to undergo protonation by solvent and subsequent pseudorotation to form migration products.[74]

Sulfur substitution at the nonbridging positions has both electronic and solvation effects. The softer sulfur atoms are able to electronically stabilize the negative charge of the dianionic thiophosphorane intermediate. However, the sulfur atoms are also larger and consequently less well solvated. The solvent effect, as will be seen in greater detail in the following sections, results in destabilization of the transition state associated with exocyclic cleavage. This is because the 5′ leaving group is partially desolvated as it leaves as an oxyanion, and this desolvation becomes exaggerated in the presence of the large nonbridging sulfur atoms. The 2′ oxygen also has to undergo desolvation when it initiates nucleophilic attack; however, this has much less of an effect on the 2′ secondary alkoxide which is more electronically stable and less solvent exposed than the 5′ primary methoxide anion.

Examination of the structures of the stationary points along on the free energy profile (Table 2) indicates that sulfur substitution at the nonbridging positions is accompanied by a contraction of the axial bonds of the intermediate and is consistent with the increased stability and lifetime of the intermediate. Sulfur substitution at the nonbridging positions results in reaction paths with increased associative character with $TS_{O_{2'}}$ and $TS_{O_{5'}}$ shifted toward reactants and products, respectively (Figure 2). The rate-limiting transition state $TS_{O_{5'}}$ becomes a later transition state with more dissociative character upon nonbridging sulfur substitution. The $TS_{O_{2'}}$ and $TS_{O_{5'}}$ have increased $r_1 = P-X_{2'}$ and $r_2 = P-X_{5'}$ distances, respectively, in the sulfur-substituted reactions relative to the native reaction. The doubly substituted reaction has the largest dissociative character for $TS_{O_{5'}}$ of all of the reactions considered here with r_1 and r_2 values of 2.49 and 2.63 Å for $TS_{O_{2'}}$ and $TS_{O_{5'}}$, respectively, relative to the corresponding values in the native reaction of 2.19 and 2.40 Å. The shift of the r_1 and r_2 values for $TS_{O_{2'}}$ and $TS_{O_{5'}}$ can be explained by the Hammond postulate:[75] sulfur substitutions preferentially stabilize the intermediate and lead to transition states $TS_{O_{2'}}$ and $TS_{O_{5'}}$ that are shifted away from the intermediate toward reactant and product, respectively.[76]

4.1.3. Substitution at 3′, 2′, and 5′ Oxygens. Sulfur substitution at the 3′ oxygen position reduces the activation energy for the reaction by 0.7 kcal/mol relative to the native structure and slightly stabilizes the intermediate. This is in contrast to the calculated results for the thio-substitutions at the nonbridging phosphoryl positions that resulted in increased rate-controlling barriers to in-line attack relative to the native reaction. The increased reaction rate predicted here for sulfur substitution at the 3′ position is consistent with the experimentally observed rate enhancement for 3′ thio-modified RNA dinucleotides. However, the calculated 3-fold increase in rate is smaller than the 200-fold[77] and 2000-fold[78] increases observed experimentally.

The slightly lower rate-controlling barrier for 3′ thio-substitution relative to the native reaction arises mainly from an electronic effect. Sulfur-substitution stabilizes the dianionic thiophosphorane intermediate electronically due to the ability of the softer sulfur to accommodate negative charge. The larger sulfur radii also reduce the degree of solvent stabilization of the intermediate. The reduced solvent stabilization for the 3′ thio-substitution is much less pronounced than that for the thio-substitutions in the nonbridging positions because the 3′ position does not carry a full −1 formal charge. The net result is that the dianionic 3′ thiophosphorane intermediate is stabilized relative to the dianionic oxyphosphorane, causing a slight shift of the r_1 and r_2 values for $TS_{O_{2'}}$ and $TS_{O_{5'}}$ toward the reactant and product, respectively, in accord with the Hammond postulate.[75] The desolvation of the $TS_{O_{5'}}$, however, is not sufficiently increased as to raise this barrier relative to the native reaction. Overall, the free energy profile for the 3′ thio-substitution is the most similar to the native reaction profile.

In contrast, thio-substitution at the 2′ or 5′ position, which represent the nucleophile and leaving groups, respectively, has a profound effect on the free energy profiles and rate-controlling activation barriers. The 2′ and 5′ thio-substituted reactions proceed through a single transition state with greatly increased and decreased rate-controlling barriers, respectively, relative to the native reaction. As discussed in the review of Jencks,[76] stabilization of the reactant tends to raise the barrier of the forward reaction and shift the reaction coordinate value of the transition state toward that of product. For product stabilization, the converse is true: the barrier of the forward reaction is reduced, and the reaction coordinate value is shifted toward that of the reactant. These effects give rise to linear free energy relationships[76] that have been applied by others to study related systems, including studies of the reactivity of phosphate monoester dianions in solution,[69] the mechanism of hydrolysis of a metal-complexed phosphate diester,[79] enzyme-catalyzed

(73) Ora, M.; Järvi, J.; Oivanen, M.; Lönnberg, H. Hydrolytic reactions of the phosphorodithioate analogue of uridylyl(3′,5′)uridine: Kinetics and mechanisms for the cleavage, desulfurization, and isomerization of the internucleosidic linkage. *J. Org. Chem.* **2000**, *65*, 2651−2657.
(74) Lopez, C. S.; Faza, O. N.; Gregersen, B. A.; López, X.; De Lera, A. R.; York, D. M. Pseudorotation of natural and chemically modified biological phosphoranes: Implications for RNA catalysis. *Chem. Phys. Chem.* **2004**, in press.
(75) Hammond, G. S. A correlation of reaction rates. *J. Am. Chem. Soc.* **1955**, *77*, 334−338.
(76) Jencks, W. P. A. Primer for the bema hapothle. An empirical approach to the characterization of changing transition-state structures. *Chem. Rev.* **1985**, *85*, 511−527.
(77) Liu, X.; Reese, C. B. 3′-Thiouridylyl-(3′→5′)-uridine. *Tetrahedron Lett.* **1996**, *37*, 925−928.
(78) Weinstein, L. B.; Earnshaw, D. J.; Cosstick, R.; Cech, T. R. Synthesis and characterization of an RNA dinucleotide containing a 3′-*S*-phosphorothiolate linkage. *J. Am. Chem. Soc.* **1996**, *118*, 10341−10350.
(79) Humphry, T.; Forconi, M.; Williams, N. H.; Hengge, A. C. An altered mechanism of hydrolysis for a metal-complexed phosphate diester. *J. Am. Chem. Soc.* **2002**, *124*, 14860−14861.

phosphoryl transfers involving the hydrolysis of O-aryl phosphorothioates,[80] and leaving group dependence in intramolecular alcoholysis of uridine 3′-aryl phosphorothioates.[81]

In the present work, the 2′ thio-substitution produces a tremendous reactant stabilization effect that leads to a large increase in the rate-controlling barrier by a factor of 2 relative to the native reaction and shifts the single transition state in the reaction profile to a $TS_{O_{5'}}$-type transition state near the product. The transition state is characterized by an almost fully formed $P-S_{2'}$ bond of 2.27 Å (Table 2). These results are consistent with experimental results on a similar 2′ thio ribonucleotide analogue[82] where the rate of thiolate attack on the phosphate center was observed to be 10^7 times slower than that of the corresponding alkoxide. While thiolates are generally more nucleophilic than alkoxides, these results demonstrate that the affinity of a 2′ thiolate toward nucleophilic attack to the phosphate center studied in the present work is significantly reduced relative to that of the corresponding 2′ alkoxide. These results are also consistent with experimental and theoretical work that suggest these reactions proceed through a single transition state with greatly reduced rate.[5,6] Although experimental data are invaluable, one must bear in mind that kinetic results may sometimes be consistent with multiple mechanistic interpretations.[83] Moreover, theoretical studies based on phosphate reaction models in the gas phase[6] are likely irrelevant for the reactions in solution.

In contrast to the 2′ thio-substitution, the 5′ thio-substitution leads to greatly increased product stabilization that lowers the rate-controlling barrier by 10.1 kcal/mol relative to the native reaction. The single transition state is shifted toward the reactant $TS_{O_{2'}}$-type corresponding to formation of the endocyclic $P-O_{2'}$ bond. These results are consistent with the increased stability of the 5′ thiolate leaving group as indicated by lower theoretical and experimental pK_a values of thiols with respect to the corresponding alcohols,[84,85] and by the experimentally observed increase in rate constants for transphosphorylation with enhanced leaving groups.[5,6,86,87]

4.2. Role of Solvation. 4.2.1. Solvation Effects on the Native Reaction. In this section, the effects of solvation on the native (unsubstituted) reaction are discussed. Subsequent discussion of solvation for the sulfur-substituted reactions will focus on how these effects differ from that of the native reaction.

Solvation of the Nucleophilic Group. The solvation of the nucleophilic 2′ alkoxide is characterized by the radial distribution function of water oxygens around the $O_{2'}$ oxygen atom (Figure 3). In the reactant state, the water oxygens in the first solvation shell around the 2′ oxygen are tightly bound and highly ordered. The first maximum and minimum in $g^{R}_{O_{2'}O_W}(r)$ for the native reaction occur at 2.8 and 3.6 Å, respectively, and have corresponding heights of 3.39 and 0.26 (Table 3). The first coordination number is 4.7, indicating that on average slightly less than 5 waters coordinate the $O_{2'}$ oxyanion in the reactant. The $g^{TS}_{O_{2'}O_W}(r)$ and $g^{P}_{O_{2'}O_W}(r)$ plots show much less pronounced first solvation layers as the reaction proceeds and the $O_{2'}$ becomes covalently bonded to the phosphorus.

Solvation around Phosphorus. The radial distribution functions around P do not change dramatically over the course of the reaction (Figure 4). The first maximum and minimum in $g^{R}_{PO_W}(r)$ for the native reaction occur at 3.9 and 4.7 Å, respectively, and have a first coordination number of 10.5. The $g^{TS}_{PO_W}(r)$ distribution exhibits an increase in the first maximum to a value of 2.3 and a corresponding change in the first coordination number to a value of 11.7 (Table 3). This increase in overall solvation around phosphorus in the transition state arises from the increase in localized charge of the dianionic oxyphosphorane relative to the charge-separated reactants and products. For the product state, the location and height of the first maximum of $g^{P}_{PO_W}(r)$ are unchanged from the reactant state. However, the coordination number (11.1) is increased relative to that of the reactant, resulting mainly from an increased rdf value at the first minimum (see Supporting Information). The interpretation for this is that the 2′,3′-cyclic phosphate product is more highly solvated around phosphorus than the acyclic phosphate reactant and the exchange rate of ordered waters decreases in the more highly ordered first solvation shell of the dianionic transition state.

Solvation of the Leaving Group. The solvation of the 5′ leaving group is characterized by the radial distribution function of water oxygens around the $O_{5'}$ atom (Figure 5). The solvation of the leaving group largely mimics that of the nucleophilic group for the reverse reaction. In the reactant state (where the 5′ oxygen is covalently bound to phosphorus), there is no discernible first solvation layer, and only slight ordering is observed between 4.5 and 5.5 Å from the 5′ oxygen. At the transition state, $g^{TS}_{O_{5'}O_W}(r)$ shows appreciable order in the first solvation layer. This is due in part to the nature of the rate-limiting transition state as that of a "late transition state" with considerable dissociative leaving group character representative of the solvated products. For the product state, there is a sharp peak at 2.8 Å in $g^{P}_{O_{5'}O_W}(r)$ with a value of 3.87, the highest peak of all the rdf's around the 5′ position (Table 3). The reason for the increased solvation around the 5′ alkoxide leaving group as compared to the 2′ nucleophile is the smaller size and increased solvent exposure of the former.

4.2.2. Effect of Nonbridging Thio-Substitution on Solvation. Single Nonbridging Thio-Substitutions. The $g^{TS}_{PO_W}(r)$ distribution is most significantly influenced by sulfur substitutions at the O_{P1} and O_{P2} oxygen positions (Figure 7). Single substitutions at either the O_{P1} or the O_{P2} oxygen cause the first maximum in the $g^{TS}_{PO_W}(r)$ to shift in position from 3.9 Å in the native reaction to 4.0 Å, and decrease in height from 2.32 in the native reaction to 1.82 and 1.74, respectively (Table 3). The first coordination number for the $g^{TS}_{PO_W}(r)$ increases by around 3.4 from 10.4 in the native reaction to 13.6−14.0 for the singly

(80) Hollfelder, F.; Herschlag, D. The nature of the transition state for enzyme-catalyzed phosphoryl transfer. Hydrolysis of O-aryl phosphorothioates by alkaline phosphatase. *Biochemistry* **1995**, *34*, 12255−12264.
(81) Almer, H.; Strömberg, R. Base catalysis and leaving group dependence in intramolecular alcoholysis of uridine 3′-(aryl phosphorothioate)s. *J. Am. Chem. Soc.* **1996**, *118*, 7921−7928.
(82) Dantzman, C. L.; Kiessling, L. L. Reactivity of a 2′-thio nucleotide analogue. *J. Am. Chem. Soc.* **1996**, *118*, 11715−11719.
(83) Åqvist, J.; Kolmodin, K.; Florian, J.; Warshel, A. Mechanistic alternatives in phosphate monoester hydrolysis: What conclusions can be drawn from available experimental data? *Chem. Biol.* **1999**, *6*, R71−R80.
(84) Silva, C. O.; Da Silva, E. C.; Nascimento, M. A. C. Ab initio calculations of absolute pka values in aqueous solution ii. aliphatic alcohols, thiols, and halogenated carboxylic acids. *J. Phys. Chem. A* **2000**, *104*, 2402−2409.
(85) Lide, D. R., Ed. *CRC Handbook of Chemistry and Physics*, 83rd ed.; CRC Press LLC: Boca Raton, FL, 2003.
(86) Liu, X.; Reese, C. B. Uridylyl-(3′→5′)-(5′-thiouridine). An exceptionally base-labile di-ribonucleoside phosphate analogue. *Tetrahedron Lett.* **1995**, *36*, 3413−3416.
(87) Thomson, J. B.; Patel, B. K.; Jiménez, V.; Eckart, K.; Eckstein, F. Synthesis and properties of diuridine phosphate analogues containing thio and amino modifications. *J. Org. Chem.* **1996**, *61*, 6273−6281.

substituted reactions, and the corresponding average coordination distance similarly increases from 4.1 to 4.4 Å.

Double Nonbridging Thio-Substitutions. In the case of double substitutions, the trends observed for the single substitutions are amplified. The location of the first maximum shifts to 4.3 Å and decreases in value to 1.43, and the first minimum shifts to 5.4 Å and increases in height to a value 0.75. An ordered second solvation shell is no longer observed. The first coordination number for the $g^{TS}_{PO_W}(r)$ increases to a value of 15.2 with an average coordination distance of 4.6 Å. The observed trend upon sulfur substitution at the nonbridging positions is to expand the first solvation layer (due to the larger size of the sulfur radii), causing a shift of the average $P-O_W$ distance and subsequent increase in number of waters in the first solvation layer. Sulfur substitutions at the O_{P1} and O_{P2} positions play a key role in determining the solvent structure around the transition state.

4.2.3. Effect of 3′, 2′, and 5′ Thio-Substitution on Solvation. Thio-Substitution at the 3′ Position. The 3′ thio-substitution has the most similarity to the native reaction of all the thio-substituted reaction profiles. The effect of 3′ substitution on solvation of the $O_{2'}$ of the reactant state and $O_{5'}$ of the product state is almost negligible. The most pronounced difference in solvation relative to that of the native reaction occurs in the transition state (Figure 7).

Thio-Substitution at the 2′ Position. Unlike the 3′ thio-substitution, the 2′ thio-substitution has a tremendous effect on the reaction profiles and solvation. The $g^{R}_{O_{2'}O_W}(r)$ (Figure 6) has a first maximum that is shifted by 0.4 Å relative to the native reaction and has an increased average coordination distance (3.38 Å) and first coordination number (6.4). The waters in the first coordination sphere are less ordered with a root-mean-square deviation in the radial distance of 2.18 Å, relative to 1.69 Å for the native reaction. Moreover, the value of $g^{R}_{O_{2'}O_W}(r)$ at the first minimum is 0.4 greater than that for the native reaction, suggesting the coordinating waters exchange more rapidly.

Thio-Substitution at the 5′ Position. The 5′ thio-substitution has the most profound effect on the series of reaction profiles studied. The 5′ thio-substitution produces a reaction profile that proceeds through a single $TS_{O_{2'}}$-type transition state and is the only reaction where the character of the rate-limiting transition state has altered from that of a $TS_{X_{5'}}$-type. The $g^{P}_{O_{5'}O_W}(r)$ has a first maximum that is shifted by 0.4 Å relative to the native reaction and has an increased average coordination distance (3.35 Å) and first coordination number (6.8) relative to the native reaction (Figure 8). This coordination number is even larger than that for the $g^{P}_{O_{2'}O_W}(r)$ of the 2′ thio-substitution reaction. The reason is that the primary 5′ thiolate is more solvent exposed than the secondary 2′ thiolate. The waters in the $g^{P}_{O_{5'}}(r)$ first coordination sphere of the 5′ thio-substituted reaction show larger radial variation and more rapid exchange than the native reaction. For the 5′ thio-substitution, the rate-limiting $TS_{O_{2'}}$-type transition state more closely resembles reactants and has a $S_{5'}-P$ bond distance ($r_2 = P-S_{5'} = 2.25$ Å) that is only slightly elongated relative to the average P−S single bond distance in the reactant state (2.05 Å).

4.2.4. New-Generation Hybrid QM/MM Potentials for RNA Catalysis. The present work is a benchmark study that investigates the role of solvation on dianionic transphosphorylation reactions of native and thio-substituted RNA model systems using a hybrid QM/MM simulation in explicit solvent. The models used in the present work have been tested against density-functional calculations[62] and have been found to be generally reliable for the dianionic reactions that do not involve intramolecular hydrogen bonding or proton transfer within the quantum subsystem.[61] Nonetheless, future work will concentrate on the design and parametrization of improved semiempirical quantum models[88−90] for reactions involved in RNA catalysis.[61] Improvements in the semiempirical form will address the problem of accurately modeling hydrogen-bonding interactions and proton-transfer reactions and also include an improved description of dispersion forces and relative conformational energies and barriers. Parametrization of these models will involve consideration of relative proton affinities of alkoxides and thiolates, phosphates and phosphorothioates, as well as reaction transition states, etc.

In addition to the quantum model, it is worthwhile to explore systematic improvements in the molecular mechanical solvation model; in particular, for dianionic reactions, the inclusion of polarization is expected to be of considerable importance. A number of recently developed polarizable models for water have been introduced that have been developed with biological simulations in mind.[91−93] For a given semiempirical quantum method and molecular mechanical solvation model, one should develop appropriate nonbonded molecular mechanical parameters for the quantum systems that accurately reproduce known experimental quantities of importance, such as the relative pK_a values of methanol and methane thiol, phosphoric acid and thiophosphoric acid, etc. Hence, there is significant room for the development of more general, robust hybrid QM/MM potentials for reactions involved in RNA catalysis. This is a focus of current work.

5. Conclusion

In this work, transphosphorylation thio effects in solution are studied using hybrid QM/MM calculations. Solvation is observed to play a key role in the reaction coordinate and profile for these reactions. The native reaction proceeds through two transition states separated by a kinetically insignificant intermediate. The transition states correspond to endocyclic bond formation and exocyclic bond cleavage, respectively, with the latter the rate-controlling transition state. The effect of sulfur substitution involves a balance of electronic and solvation effects. For the nonbridging thio-substitutions, the softer sulfur atoms better electronically stabilize the dianionic intermediate; however, that larger radius of sulfur causes decreased solvent stabilization of the primary 5′ methoxide leaving group that

(88) Thiel, W. Perspectives on semiempirical molecular orbital theory. In *Advances in Chemical Physics*; Prigogine, I., Rice, S. A., Eds.; John Wiley and Sons: New York, 1996; Vol. 93, pp 703−757.
(89) Clark, T. Quo vadis semiempirical MO-theory? *J. Mol. Struct. (THEOCHEM)* **2000**, *530*, 1−10.
(90) Winget, P.; Selcuki, C.; Horn, A. H. C.; Martin, B.; Clark, T. Towards a "next generation" neglect of diatomic differential overlap based semi-empirical molecular orbital technique. *Theor. Chem. Acc.* **2003**, *110*, 254−266.
(91) Stern, H. A.; Rittner, F.; Berne, B. J.; Friesner, R. A. Combined fluctuating charge and polarizable dipole models: Application to a five-site water potential function. *J. Chem. Phys.* **2001**, *115*, 2237−2251.
(92) Ren, P.; Ponder, J. W. Polarizable atomic multipole water model for molecular mechanics simulation. *J. Phys. Chem. B* **2003**, *107*, 5933−5947.
(93) Lamoureux, G.; Mackerell, A. D., Jr.; Roux, B. A simple polarizabile model of water based on classical Drude oscillators. *J. Chem. Phys.* **2003**, *119*, 5185−5197.

raises the rate-controlling barrier. An interesting feature of these reaction profiles is the existence of a stable dianionic thiophosphorane intermediate that, especially in the case of the double nonbridging thio-substitution, is predicted to have significant lifetime that might be sufficient to undergo protonation by solvent and subsequent pseudorotation. Thio-substitution at the 3′ bridging position has the smallest effect on the reaction profile and slightly lowers the rate-controlling barrier. In contrast, thio-substitution at the 2′ and 5′ positions, corresponding to the nucleophile and leaving group, respectively, has a dramatic effect. The reaction profiles for these reactions proceed through a single transition state. The 2′ thio-substitution raises the rate-controlling barrier by a factor of 2. The activated 2′ thiolate is a more stable species than the corresponding 2′ alkoxide, and hence 2′ thio-substitution results in reactant stabilization (reduction in nucleophilicity) and an increased forward barrier. The 5′ thio-substitution, on the other hand, greatly enhances the acyclic 5′ leaving group ability that, in the native reaction, is the rate-controlling barrier. The 5′ thio-substitution shifts the character of the transition state to that of the endocyclic bond formation and greatly reduces the rate-controlling barrier of the reaction by around 10 kcal/mol.

The hybrid QM/MM potential and simulation protocol tested and applied in the present work provide overall trends that agree well with experiment. Nonetheless, there is considerable room for the design of improved hybrid QM/MM potentials that combine more accurate quantum models for specific reactions with improved forms of the molecular mechanical model to represent the environment. The design of such potentials would provide a powerful tool that, in conjunction with experimental methods, may offer detailed atomic-level insight into the catalytic mechanisms of ribozymes and phosphoryl transfer reactions mediated by kinase and phosphatase signaling proteins. The present work represents a benchmark test of the limits in accuracy of existing state-of-the-art hybrid QM/MM methods and an important step in the progress toward the development of improved computational models for the study of RNA catalysis.

Acknowledgment. D.M.Y. is grateful for financial support provided by the National Institutes of Health (Grant 1R01-GM62248-01A1), and the Army High Performance Computing Research Center (AHPCRC) under the auspices of the Department of the Army, Army Research Laboratory (ARL) under Cooperative Agreement number DAAD19-01-2-0014. X.L. thanks the MSI for a Research Scholar Award, the Basque Government (Eusko Jaurlaritza), and the University of the Basque Country (Euskal Herriko Unibersitatea) for financial support. Computational resources were provided by the Minnesota Supercomputing Institute.

Supporting Information Available: Radial distribution statistics for water oxygens around $O_{2'}$, $O_{5'}$, $O_{3'}$, O_{P1}, O_{P2}, and P are provided for the reactant, transition, and product states. This material is available free of charge via the Internet at http://pubs.acs.org.

JA031815L